Production of excited beauty states in Z decays

D. Buskulic, D. Casper, I. de Bonis, D. Decamp, P. Ghez, C. Goy, J.P. Lees, A. Lucotte, M.N. Minard, P. Odier, et al.

EUROPEAN ORGANISATION FOR NUCLEAR RESEARCH

CERN-PPE/95-108
14 July 1995

Production of Excited Beauty States in Z Decays

The ALEPH Collaboration

Abstract

A data sample of about 3.0 million hadronic Z decays collected by the ALEPH experiment at LEP in the years 1991 through 1994, is used to make an inclusive selection of B hadron events. In this event sample $4227 \pm 140 \pm 252$ B^* mesons in the decay $B^* \to B\gamma$ and $1944 \pm 108 \pm 161$ B^{**} mesons decaying into a B meson and a charged pion are reconstructed. For the well established B^* meson the following quantities are obtained: $\Delta M = M_{B^*} - M_B = (45.30 \pm 0.35 \pm 0.87)$ MeV/c^2 and $N_{B^*}/(N_B + N_{B^*}) = (77.1 \pm 2.6 \pm 7.0)\%$. The angular distribution of the photons in the B^* rest frame is used to measure the relative contribution of longitudinal B^* polarization states to be $\sigma_L/(\sigma_L + \sigma_T) = (33 \pm 6 \pm 5)\%$.
Resonance structure in the $M(B\pi) - M(B)$ mass difference is observed at $(424 \pm 4 \pm 10)$ MeV/c^2. Its shape and position is in agreement with the expectation for $B^{**}_{u,d}$ states decaying into $B^{(*)}_{u,d}\pi^{\pm}$. The signal is therefore interpreted as arising from them. The relative production rate is determined to be

$$\frac{BR(Z \to b \to B^{**}_{u,d})}{BR(Z \to b \to B_{u,d})} = [27.9 \pm 1.6(stat) \pm 5.9(syst)\ {}^{+3.9}_{-5.6}(model)]\%.$$

where the third error reflects the uncertainty due to different production and decay models for the broad $B^{**}_{u,d}$ states.

(Submitted to Zeitschrift für Physik C)

The ALEPH Collaboration

D. Buskulic, D. Casper, I. De Bonis, D. Decamp, P. Ghez, C. Goy, J.-P. Lees, A. Lucotte, M.-N. Minard, P. Odier, B. Pietrzyk

Laboratoire de Physique des Particules (LAPP), IN^{2}P^3-CNRS, 74019 Annecy-le-Vieux Cedex, France

F. Ariztizabal, M. Chmeissani, J.M. Crespo, I. Efthymiopoulos, E. Fernandez, M. Fernandez-Bosman, V. Gaitan, Ll. Garrido,[15] M. Martinez, S. Orteu, A. Pacheco, C. Padilla, F. Palla, A. Pascual, J.A. Perlas, F. Sanchez, F. Teubert

Institut de Fisica d'Altes Energies, Universitat Autonoma de Barcelona, 08193 Bellaterra (Barcelona), Spain[7]

A. Colaleo, D. Creanza, M. de Palma, A. Farilla, G. Gelao, M. Girone, G. Iaselli, G. Maggi,[3] M. Maggi, N. Marinelli, S. Natali, S. Nuzzo, A. Ranieri, G. Raso, F. Romano, F. Ruggieri, G. Selvaggi, L. Silvestris, P. Tempesta, G. Zito

Dipartimento di Fisica, INFN Sezione di Bari, 70126 Bari, Italy

X. Huang, J. Lin, Q. Ouyang, T. Wang, Y. Xie, R. Xu, S. Xue, J. Zhang, L. Zhang, W. Zhao

Institute of High-Energy Physics, Academia Sinica, Beijing, The People's Republic of China[8]

G. Bonvicini, M. Cattaneo, P. Comas, P. Coyle, H. Drevermann, A. Engelhardt, R.W. Forty, M. Frank, R. Hagelberg, J. Harvey, R. Jacobsen,[24] P. Janot, B. Jost, J. Knobloch, I. Lehraus, C. Markou,[23] E.B. Martin, P. Mato, H. Meinhard, A. Minten, R. Miquel, T. Oest, P. Palazzi, J.R. Pater,[27] J.-F. Pusztaszeri, F. Ranjard, P. Rensing, L. Rolandi, D. Schlatter, M. Schmelling, O. Schneider, W. Tejessy, I.R. Tomalin, A. Venturi, H. Wachsmuth, W. Wiedenmann, T. Wildish, W. Witzeling, J. Wotschack

European Laboratory for Particle Physics (CERN), 1211 Geneva 23, Switzerland

Z. Ajaltouni, M. Bardadin-Otwinowska,[2] A. Barres, C. Boyer, A. Falvard, P. Gay, C. Guicheney, P. Henrard, J. Jousset, B. Michel, S. Monteil, J-C. Montret, D. Pallin, P. Perret, F. Podlyski, J. Proriol, J.-M. Rossignol, F. Saadi

Laboratoire de Physique Corpusculaire, Université Blaise Pascal, IN^{2}P^3-CNRS, Clermont-Ferrand, 63177 Aubière, France

T. Fearnley, J.B. Hansen, J.D. Hansen, J.R. Hansen, P.H. Hansen, B.S. Nilsson

Niels Bohr Institute, 2100 Copenhagen, Denmark[9]

A. Kyriakis, E. Simopoulou, I. Siotis, A. Vayaki, K. Zachariadou

Nuclear Research Center Demokritos (NRCD), Athens, Greece

A. Blondel,[21] G. Bonneaud, J.C. Brient, P. Bourdon, L. Passalacqua, A. Rougé, M. Rumpf, R. Tanaka, A. Valassi,[31] M. Verderi, H. Videau

Laboratoire de Physique Nucléaire et des Hautes Energies, Ecole Polytechnique, IN^{2}P^3-CNRS, 91128 Palaiseau Cedex, France

D.J. Candlin, M.I. Parsons

Department of Physics, University of Edinburgh, Edinburgh EH9 3JZ, United Kingdom[10]

E. Focardi, G. Parrini

Dipartimento di Fisica, Università di Firenze, INFN Sezione di Firenze, 50125 Firenze, Italy

M. Corden, M. Delfino,[12] C. Georgiopoulos, D.E. Jaffe

Supercomputer Computations Research Institute, Florida State University, Tallahassee, FL 32306-4052, USA [13,14]

A. Antonelli, G. Bencivenni, G. Bologna,[4] F. Bossi, P. Campana, G. Capon, V. Chiarella, G. Felici, P. Laurelli, G. Mannocchi,[5] F. Murtas, G.P. Murtas, M. Pepe-Altarelli

Laboratori Nazionali dell'INFN (LNF-INFN), 00044 Frascati, Italy

S.J. Dorris, A.W. Halley, I. ten Have,[6] I.G. Knowles, J.G. Lynch, W.T. Morton, V. O'Shea, C. Raine, P. Reeves, J.M. Scarr, K. Smith, M.G. Smith, A.S. Thompson, F. Thomson, S. Thorn, R.M. Turnbull

Department of Physics and Astronomy, University of Glasgow, Glasgow G12 8QQ,United Kingdom[10]

U. Becker, O. Braun, C. Geweniger, G. Graefe, P. Hanke, V. Hepp, E.E. Kluge, A. Putzer, B. Rensch, M. Schmidt, J. Sommer, H. Stenzel, K. Tittel, S. Werner, M. Wunsch

Institut für Hochenergiephysik, Universität Heidelberg, 69120 Heidelberg, Fed. Rep. of Germany[16]

R. Beuselinck, D.M. Binnie, W. Cameron, D.J. Colling, P.J. Dornan, N. Konstantinidis, L. Moneta, A. Moutoussi, J. Nash, G. San Martin, J.K. Sedgbeer, A.M. Stacey

Department of Physics, Imperial College, London SW7 2BZ, United Kingdom[10]

G. Dissertori, P. Girtler, E. Kneringer, D. Kuhn, G. Rudolph

Institut für Experimentalphysik, Universität Innsbruck, 6020 Innsbruck, Austria[18]

C.K. Bowdery, T.J. Brodbeck, P. Colrain, G. Crawford, A.J. Finch, F. Foster, G. Hughes, T. Sloan, E.P. Whelan, M.I. Williams

Department of Physics, University of Lancaster, Lancaster LA1 4YB, United Kingdom[10]

A. Galla, A.M. Greene, K. Kleinknecht, G. Quast, J. Raab, B. Renk, H.-G. Sander, R. Wanke, C. Zeitnitz

Institut für Physik, Universität Mainz, 55099 Mainz, Fed. Rep. of Germany[16]

J.J. Aubert, A.M. Bencheikh, C. Benchouk, A. Bonissent,[21] G. Bujosa, D. Calvet, J. Carr, C. Diaconu, F. Etienne, M. Thulasidas, D. Nicod, P. Payre, D. Rousseau, M. Talby

Centre de Physique des Particules, Faculté des Sciences de Luminy, IN^{2}P^3-CNRS, 13288 Marseille, France

I. Abt, R. Assmann, C. Bauer, W. Blum, D. Brown,[24] H. Dietl, F. Dydak,[21] G. Ganis, C. Gotzhein, K. Jakobs, H. Kroha, G. Lütjens, G. Lutz, W. Männer, H.-G. Moser, R. Richter, A. Rosado-Schlosser, S. Schael, R. Settles, H. Seywerd, U. Stierlin,[2] R. St. Denis, G. Wolf

Max-Planck-Institut für Physik, Werner-Heisenberg-Institut, 80805 München, Fed. Rep. of Germany[16]

R. Alemany, J. Boucrot, O. Callot, A. Cordier, F. Courault, M. Davier, L. Duflot, J.-F. Grivaz, Ph. Heusse, M. Jacquet, D.W. Kim,[19] F. Le Diberder, J. Lefrançois, A.-M. Lutz, G. Musolino, I. Nikolic, H.J. Park, I.C. Park, M.-H. Schune, S. Simion, J.-J. Veillet, I. Videau

Laboratoire de l'Accélérateur Linéaire, Université de Paris-Sud, IN^{2}P^3-CNRS, 91405 Orsay Cedex, France

D. Abbaneo, P. Azzurri, G. Bagliesi, G. Batignani, S. Bettarini, C. Bozzi, G. Calderini, M. Carpinelli, M.A. Ciocci, V. Ciulli, R. Dell'Orso, R. Fantechi, I. Ferrante, L. Foà,[1] F. Forti, A. Giassi, M.A. Giorgi, A. Gregorio, F. Ligabue, A. Lusiani, P.S. Marrocchesi, A. Messineo, G. Rizzo, G. Sanguinetti, A. Sciabà, P. Spagnolo, J. Steinberger, R. Tenchini, G. Tonelli,[26] G. Triggiani, C. Vannini, P.G. Verdini, J. Walsh

Dipartimento di Fisica dell'Università, INFN Sezione di Pisa, e Scuola Normale Superiore, 56010 Pisa, Italy

A.P. Betteridge, G.A. Blair, L.M. Bryant, F. Cerutti, Y. Gao, M.G. Green, D.L. Johnson, T. Medcalf, Ll.M. Mir, P. Perrodo, J.A. Strong

Department of Physics, Royal Holloway & Bedford New College, University of London, Surrey TW20 OEX, United Kingdom[10]

V. Bertin, D.R. Botterill, R.W. Clifft, T.R. Edgecock, S. Haywood, M. Edwards, P. Maley, P.R. Norton, J.C. Thompson

Particle Physics Dept., Rutherford Appleton Laboratory, Chilton, Didcot, Oxon OX11 OQX, United Kingdom[10]

B. Bloch-Devaux, P. Colas, H. Duarte, S. Emery, W. Kozanecki, E. Lançon, M.C. Lemaire, E. Locci, B. Marx, P. Perez, J. Rander, J.-F. Renardy, A. Rosowsky, A. Roussarie, J.-P. Schuller, J. Schwindling, D. Si Mohand, A. Trabelsi, B. Vallage

CEA, DAPNIA/Service de Physique des Particules, CE-Saclay, 91191 Gif-sur-Yvette Cedex, France[17]

R.P. Johnson, H.Y. Kim, A.M. Litke, M.A. McNeil, G. Taylor

Institute for Particle Physics, University of California at Santa Cruz, Santa Cruz, CA 95064, USA[22]

A. Beddall, C.N. Booth, R. Boswell, S. Cartwright, F. Combley, I. Dawson, A. Koksal, M. Letho, W.M. Newton, C. Rankin, L.F. Thompson

Department of Physics, University of Sheffield, Sheffield S3 7RH, United Kingdom[10]

A. Böhrer, S. Brandt, G. Cowan, E. Feigl, C. Grupen, G. Lutters, J. Minguet-Rodriguez, F. Rivera,[25] P. Saraiva, L. Smolik, F. Stephan, P. van Gemmeren

Fachbereich Physik, Universität Siegen, 57068 Siegen, Fed. Rep. of Germany[16]

M. Apollonio, L. Bosisio, R. Della Marina, G. Giannini, B. Gobbo, F. Ragusa[20]

Dipartimento di Fisica, Università di Trieste e INFN Sezione di Trieste, 34127 Trieste, Italy

J. Rothberg, S. Wasserbaech

Experimental Elementary Particle Physics, University of Washington, WA 98195 Seattle, U.S.A.

S.R. Armstrong, L. Bellantoni,[30] P. Elmer, Z. Feng, D.P.S. Ferguson, Y.S. Gao, S. González, J. Grahl, J.L. Harton,[28] O.J. Hayes, H. Hu, P.A. McNamara III, J.M. Nachtman, W. Orejudos, Y.B. Pan, Y. Saadi, M. Schmitt, I.J. Scott, V. Sharma,[29] J.D. Turk, A.M. Walsh, Sau Lan Wu, X. Wu, J.M. Yamartino, M. Zheng, G. Zobernig

Department of Physics, University of Wisconsin, Madison, WI 53706, USA[11]

---

[1] Now at CERN, 1211 Geneva 23, Switzerland.
[2] Deceased.
[3] Now at Dipartimento di Fisica, Università di Lecce, 73100 Lecce, Italy.
[4] Also Istituto di Fisica Generale, Università di Torino, Torino, Italy.
[5] Also Istituto di Cosmo-Geofisica del C.N.R., Torino, Italy.
[6] Now at TSM Business School, Enschede, The Netherlands.
[7] Supported by CICYT, Spain.
[8] Supported by the National Science Foundation of China.
[9] Supported by the Danish Natural Science Research Council.
[10] Supported by the UK Particle Physics and Astronomy Research Council.
[11] Supported by the US Department of Energy, grant DE-FG0295-ER40896.
[12] On leave from Universitat Autonoma de Barcelona, Barcelona, Spain.
[13] Supported by the US Department of Energy, contract DE-FG05-92ER40742.
[14] Supported by the US Department of Energy, contract DE-FC05-85ER250000.
[15] Permanent address: Universitat de Barcelona, 08208 Barcelona, Spain.
[16] Supported by the Bundesministerium für Forschung und Technologie, Fed. Rep. of Germany.
[17] Supported by the Direction des Sciences de la Matière, C.E.A.
[18] Supported by Fonds zur Förderung der wissenschaftlichen Forschung, Austria.
[19] Permanent address: Kangnung National University, Kangnung, Korea.
[20] Now at Dipartimento di Fisica, Università di Milano, Milano, Italy.
[21] Also at CERN, 1211 Geneva 23, Switzerland.
[22] Supported by the US Department of Energy, grant DE-FG03-92ER40689.
[23] Now at University of Athens, 157-71 Athens, Greece.
[24] Now at Lawrence Berkeley Laboratory, Berkeley, CA 94720, USA.
[25] Partially supported by Colciencias, Colombia.
[26] Also at Istituto di Matematica e Fisica, Università di Sassari, Sassari, Italy.
[27] Now at Schuster Laboratory, University of Manchester, Manchester M13 9PL, UK.
[28] Now at Colorado State University, Fort Collins, CO 80523, USA.
[29] Now at University of California at San Diego, La Jolla, CA 92093, USA.
[30] Now at Fermi National Accelerator Laboratory, Batavia, IL 60510, USA.
[31] Supported by the Commission of the European Communities, contract ERBCHBICT941234.

1 Introduction

The low lying $B(1S)$ states, B and B^*, are well established [1]. From spin counting the relative production rate of B^* mesons is expected to be $N_{B^*}/(N_B + N_{B^*}) = 0.75$ [1]. The analogous quantity measured in the charm sector is 0.51 ± 0.04 [2] in contradiction to the expectation. Phase space corrections due to the different masses of the excited- and ground states and the decay modes of the tensor meson states are possible explanations for the observed value. Measurements of the B^* and B^{**} production rates and of the B^{**} branching ratios to $B\pi$ and $B^*\pi$ are needed in order to test the prediction of 0.75 in the beauty sector.

The fraction of b quarks forming a B^{**} state is also of great interest since their expected decay modes into $B^{(*)}\pi^{\pm}$ can be used to identify the flavour of the b quark at the production time. A method based on this idea has been proposed to measure CP-violation in the decay of the neutral B meson [4]. Due to this proposal much effort was made to predict the properties of the B^{**} states based on extrapolations from the K^{**} and D^{**} sectors [4] [5]. They are summarized in table 1. The predicted masses and widths of the two narrow $B^{**}_{u,d}$ states B_1 $[B(1^+_{3/2})]$ and B^*_2 $[B(2^+_{3/2})]$ are similar while the $j = 1/2$ states are expected about 100 MeV/c^2 lower [4] and to be broad.

The recent experimental data on the D_1 and D^*_2 production rate [3] suggest a value for $BR(c \to D^{**})$ of the order of 20%. If a similar value holds for $BR(b \to B^{**})$ a clear signal for the decay $B^{**} \to B^{(*)}\pi^{\pm}$ should be visible in the large B hadron sample collected by the ALEPH experiment.

Due to the small mass splitting between B^* and B mesons only electromagnetic decays of the B^* to $B\gamma$ are allowed. The photons from the B^* decay are very low energy; with a mean of ≈ 0.3 GeV and a maximum energy of 0.8 GeV. Therefore instead of using the electromagnetic calorimeter (ECAL), which has a limited resolution and efficiency in this low energy region, the tracking system is used to reconstruct and identify converted photons. The B^* mass and production rate is measured using a reconstruction method in which these converted photons are associated to selected b jets. The B meson momentum and direction is estimated by assigning particles inside the jet to either the primary or B decay vertex according to their impact parameter and rapidity relative to the jet axis. The technique is extended to a search for B^{**} states by replacing the photon with a charged particle.

[1] Throughout the paper N_B and N_{B^*} refer to the number of primary $B^{(*)}$ mesons.

	$q = u, d$			$q = s$		
State (J^P_j)	Mass (GeV/c^2)	Width (GeV)	Decay mode	Mass (GeV/c^2)	Width (GeV)	Decay modes
$1^+_{3/2}$	5.76	0.020	$(B^*\pi)_{l=2}$	5.83	< 0.001	$(B^*K)_{l=2}$
$0^+_{1/2}$	≈ 5.65	broad	$(B\pi)_{l=0}$	≈ 5.74		$(BK)_{l=0}$, $B^*_s\gamma$
$1^+_{1/2}$	≈ 5.65	broad	$(B^*\pi)_{l=0}$	≈ 5.74		$B_s\gamma$, $B^*_s\gamma$
$2^+_{3/2}$	5.77	0.024	$(B^*\pi)_{l=2}$, $(B\pi)_{l=2}$	5.85	0.002	$(BK)_{l=2}$, $(B^*K)_{l=2}$

Table 1: Expected properties of L = 1 $b\bar{q}$ states.

2 The ALEPH detector and Data Sample

The ALEPH detector is described in detail elsewhere [6]. Only a brief description of the apparatus is given here. Charged particles are tracked with three devices inside a superconducting solenoid which provides an axial field of 1.5 Tesla. Closest to the beampipe is the vertex detector (VDET), installed in 1991, which consists of silicon wafers with strip readout in two dimensions, arranged in two cylindrical layers at average radii 6.3 and 10.8 cm. This detector covers an angular range down to $|\cos\theta| < 0.85$ for the inner layer and $|\cos\theta| < 0.69$ for the outer layer. The point resolution is $12\mu m$ at normal incidence in the $r\phi$ and z coordinates. Surrounding the VDET is the inner tracking chamber (ITC), a drift chamber giving up to eight measurements in $r\phi$. Outside the ITC, the time projection chamber (TPC) provides up to 21 space points for $|\cos\theta| < 0.79$, and a decreasing number of points for smaller angles, with four at $|\cos\theta| = 0.96$. For tracks measured by all three devices a momentum resolution of $\Delta p/p = 0.0006p$ (GeV/c)$^{-1}$ is obtained for 45 GeV/c muons. The TPC also gives up to 338 measurements of the specific ionization of each charged track, with a measured dE/dx resolution of 4.5% for Bhabha electrons having 338 ionization samples.

The ECAL was used in combination with the hadronic calorimeter (HCAL) to measure the energy of neutral particles produced in hadronic Z decays to reconstruct the B-hadron momentum.

A total sample of 3 million hadronic Z decays recorded by the ALEPH detector in the years 1991 through 1994 is used in this analysis. The Monte Carlo simulation used to determine efficiencies and estimate backgrounds is based on DYMU3 [8] and the JETSET 7.3 parton shower Monte Carlo [9]. The decay modes of the B- and D-hadrons are adjusted to agree with the most recent experimental results. A lifetime of 1.5 ps is assumed for all B hadrons. Detector effects are simulated with a detailed model of the material and detector response, based on the GEANT 3.15 package [10].

3 Selection and Reconstruction of B hadrons

B hadrons are tagged using the algorithm described in Ref.[11], in which the impact parameters of charged tracks are used to select long lived particles. In a first step the events are divided into jets using the JADE algorithm [12] with a y-cut of 0.01. Then the probability $\mathcal{P}_T$ for a charged track to belong to the primary vertex based on its signed impact parameter is calculated. This is the input to compute for each jet the probability $\mathcal{P}_J$ that a given collection of tracks has no decay products from long-lived particles. Requiring $\mathcal{P}_J$ to be less than a given value increases the likelihood that the event contains long-lived particles. The jet probabilities $\mathcal{P}_J$ are combined to form an event probability $\mathcal{P}_E$. As only the relative production rates of B^* and B^{**} mesons per B meson are determined, the value of the b purity estimated from the Monte Carlo simulation is sufficient while the absolute B tagging efficiency is not needed. Due to the different requirements of the $B^* \to B\gamma$ and $B^{**} \to B^{(*)}\pi^{\pm}$ searches, different cuts on $\mathcal{P}_E$ and $\mathcal{P}_J$ are used (section 5 and 6). But in both cases the analysis is performed in a preselected sample of B events with a purity of 88%, a sample which was also used to develop a method for the inclusive reconstruction of B hadrons.

For charged particles two quantities are used to decide whether they belong to the primary vertex or the B decay vertex: the track probability $\mathcal{P}_T$ as obtained from the signed impact parameter and the rapidity computed relative to the jet axis. The different rapidity distributions for particles from B decays compared to particles from the primary fragmentation process (see Fig. 1a) can also be used to classify neutral particles. For this purpose the pion mass is assigned to all charged particles while the neutrals are treated as massless. A simple cut in $\mathcal{P}_T$ $(-0.05 \leq \mathcal{P}_T \leq 0.2)$ [2] and in rapidity is used to decide whether a particle in the jet belongs to the B hadron or not. From Monte Carlo studies it is found that the best resolution on the B hadron direction and momentum is achieved by placing this cut at a rapidity value of 1.6 for charged and neutral tracks. In order to reduce poorly measured B jets a reconstructed B hadron mass (Fig. 1b) between 2 and 10 GeV/c^2 and a measured jet energy normalized to the beam energy (Fig. 1c) between 0.4 and 1.4 is required.

To account for neutrino losses, detector inefficiencies and wrong mass assignments a correction dependent on the measured B hadron mass and relative jet energy is applied, as determined from the Monte Carlo simulation. This improves the relative B momentum resolution significantly, although for B jets with a low estimate for the B hadron momentum the resolution for the direction and the momentum is still poor. A minimum reconstructed B hadron momentum of $p_B > 25$ GeV/c is therefore required. With this procedure one finds for the remaining B hadrons a momentum resolution function with an rms of 17.6%. 70% of the B hadrons have a momentum resolution of 9% while the rest constitute a non-Gaussian tail towards higher estimated momenta. The resolution function for the B direction can be parameterized by a double Gaussian with rms widths of 14 mrad for 80% of the B hadrons and 36 mrad for the remaining 20%.

A comparison of the reconstructed B hadron momentum spectrum in data and Monte Carlo is shown in Fig. 1d. While both distributions have the same mean value the shapes are slightly different. The Monte Carlo events are therefore reweighted to match the data and the resulting difference in masses and production rates of B^* and B^{**} mesons is included in the systematic errors.

4 Reconstruction of Converted Photons

The probability for photon conversions in the material in front of the ECAL varies from $\sim$ 7% at 90° to the beam axis to $\sim$ 10% at 30°. The material in the VDET detector and at the ITC-TPC wall are the two dominant sources for photon conversions.

In a first step a general V^0 search in the event is applied [11]. Reconstructed V^0's are identified according to their mass as K^0's, Λ's or photons. In a next step the knowledge that most of the converted photons should have their origin close to the primary vertex is used to increase the reconstruction efficiency compared to the general V^0 search. The geometrical signature for an electron or positron to originate from a photon conversion is a point (R, θ, ϕ) along its reconstructed track where the tangent is pointing to the photon production point, which is for this analysis the event main vertex (see Fig. 2a). All such tracks in an event are selected. Pairs of oppositely charged tracks which fulfill the following criteria are accepted to originate from a converted photon:

[2] The sign is given to $\mathcal{P}_T$ according to the sign of the impact parameter.

- The two conversion points (R_i, θ_i, ϕ_i) fulfill $|\theta_1 - \theta_2| \leq 0.2$ rad and $|\phi_1 - \phi_2| \leq 0.4$ rad.
- The mean conversion radius, $(R_1 + R_2)/2$, is larger than 4 cm and less than 140 cm.
- At least one of the two tracks has no measured coordinate between the interaction point and the mean conversion point.
- If particle identification information is available from dE/dx it has to be compatible (probability $> 0.1\%$) for at least one of the two tracks with the electron hypothesis.

Corrections are applied to the photon energy for the energy loss of the electron and positron in the material between the conversion point and the TPC. The relative energy resolution of the accepted pairs is 2.0% and the angular resolution is 2 mrad in θ and ϕ.

For low energy photons, which are of special interest for this analysis, it is very likely that only one track from the conversion electron-positron pair has a large enough momentum to be seen in the TPC. Therefore in the third step those tracks which pass the following cuts are accepted as originating from a photon conversion:

- The significance of the conversion point to be different from the main vertex is at least 2 sigma.
- If particle identification information is available from dE/dx it has to be compatible (probability $> 0.1\%$) with the electron hypothesis.
- If the electron probability from the dE/dx measurement is less than 10% the conversion radius has to be larger than 10 cm.
- The track has no measured coordinate between the interaction point and the conversion point.

The direction of the photon is determined by the conversion point (R, θ, ϕ) with a precision of 4 mrad in θ and ϕ. For the lost track from the electron-positron conversion pair an energy correction of 72 MeV/$\sin\theta$ is applied, as determined from the Monte Carlo simulation. In the same way as for the conversion pairs the energy loss due to the material between the conversion point and the TPC is corrected. The relative energy resolution for the conversions reconstructed from only a single track is $\approx 10\%$.

The calibration of the converted photons is tested in data and Monte Carlo using photons from π^0 decays. The $\gamma\gamma$ invariant mass spectrum is shown in Fig. 2b using two converted photons. One photon is fully reconstructed and for the second photon an energy of less than 1 GeV is required in order to have a similar sample composition as for the $B^* \to B\gamma$ analysis. The measured π^0 mass is $(134.7 \pm 0.8 \pm 1.9)$ MeV/c^2, in agreement with the expected value. The systematic error reflects the uncertainty due to the choice of the background parametrization. The total error of 1.5% is used as an absolute systematic error on the γ energy scale in the $B^* \to B\gamma$ analysis.

The efficiency to reconstruct a photon conversion as a function of energy is shown in Fig. 2c. The purity is nearly 90%. The radial distribution of conversion points in data and Monte Carlo is shown in Fig. 2d. The absolute rate of reconstructed converted photons in data and Monte Carlo differ by $[0.1 \pm 0.5(\text{stat.})]\%$.

5 The decay $B^* \to B\gamma$

Events enriched in B hadrons are selected by requiring an event probability of $\mathcal{P}_E \leq 4.0 \times 10^{-4}$ according to the lifetime tag algorithm [11]. For jets which in addition passed the B hadron momentum reconstruction as discussed in section 3, a b quark purity of 94% is obtained from the Monte Carlo simulation.

In these events the reconstructed B momentum vectors are combined with all converted photons which have an angle α relative to the B meson direction satisfying $\cos\alpha \geq 0.8$ and an energy between 0.2 and 3 GeV. To reduce the combinatorial background a cut on the photon helicity angle in the B^* rest frame, $\cos\theta^*_\gamma \geq 0$, is applied. A flat distribution is expected for photons from $B^* \to B\gamma$ decay (see section 5.2), while the combinatorial background peaks in this distribution at -1. In the Monte Carlo simulation event samples with B^*-B mass differences between 46 and 58 MeV/c^2 were generated. The reconstructed B^* mass is always within 1σ (statistical error only) of the nominal value.

The $B\gamma$-B-mass distribution obtained from 1991–1994 data is shown in Fig. 3. The expected background from the Monte Carlo simulation is shown as a hatched area scaled to the same number of $q\bar{q}$-events. The background is dominated by photons from π^0 decays. No particular source of neutral pions dominates the background. The inclusive π^0 momentum spectrum in Z decays is described well [13] by the JETSET program used in the ALEPH Monte Carlo simulation.

Converted photons can be measured down to energies of 200 MeV. This allows a comparison of the background shape in data and Monte Carlo on both sides of the peak. The background-subtracted distribution (Fig. 3b) can be approximated by a simple Gaussian. The fitted number of B^* mesons is

$$N(B^*) = 4227 \pm 140 \pm 252. \tag{1}$$

The B^*-B-mass splitting is measured to be

$$\Delta M = M(B^*) - M(B) = (45.30 \pm 0.35 \pm 0.87)\ \text{MeV/c}^2. \tag{2}$$

The systematic errors arise from the following sources:

- The difference in the reconstructed B hadron momentum spectrum (Fig. 1d) in data and Monte Carlo and the discrepancy of the photon spectra obtained in the sideband region of the B^* signal is used to reweight the Monte Carlo events to match the data. For photon energies between 0.2 and 1.0 GeV excellent agreement between the photon spectrum in data and Monte Carlo is observed while the maximum deviation at higher photon energies is 10% at 3 GeV. The systematic uncertainty on $N(B^*)$ obtained is ± 215, and the effect on ΔM is negligible.

- The limited Monte Carlo statistics for the background subtraction results in a systematic error of ± 132 on $N(B^*)$ and $\pm$ 0.3 MeV/c^2 on ΔM.

- The variation of the required reconstructed minimum B momentum between 20 and 30 GeV/c causes a variation in ΔM by ± 0.4 MeV/c^2. The effect on the relative B^* production rate is discussed in section 5.1.

- A systematic error of 1.5% is assigned to the absolute energy scale of the reconstructed photons from the study of the π^0 signal.

The rms width of the resulting B^* signal is (9.4 ± 0.5) MeV/c^2 in data and (9.8 ± 0.5) MeV/c^2 in Monte Carlo. It is dominated for conversion pairs by the measurement of the B meson direction. For conversions reconstructed only from a single track, which account for $\approx 75\%$ of the signal, the energy and direction resolution of the photon and B meson contribute similarly to the width of the B^* signal. Within the experimental resolution it is not possible to separate the B_u^*, B_d^* and B_s^* states, thus the quoted numbers are an average weighted by the production rates of the B^* states.

5.1 B^* production rate

The measured number of B^* mesons, $N(B^*)$, is related to the relative production rate of B^* mesons in Z decays by the following expression:

$$N(B^*) = N_{TAG}\ \eta_B\ \epsilon_\gamma\ f_B\ \frac{N_{B^*}}{N_B + N_{B^*}} \tag{3}$$

where N_{TAG} is the number of tagged B jets, η_B is the b event purity, ϵ_γ is the photon reconstruction efficiency, f_B is the fraction of B mesons produced in $Z \to b\bar{b}$ decays estimated to be $f_B = (87.8 \pm 4.3)\%$ [14] and $N_{B^*}/(N_B + N_{B^*})$ is the relative production probability of vector B mesons.

From a data sample of $N_{q\bar{q}} = 2,948,727$ candidate $q\bar{q}$ events $N_{TAG} = 462,204$ B jets are selected in which $4227 \pm 140 \pm 252$ B^* mesons are reconstructed. With the photon conversion and reconstruction probability $\epsilon_\gamma = (1.44 \pm 0.04)\%$ and the b purity $\eta_B = (94 \pm 2)\%$ taken from the Monte Carlo simulation, a relative B^* production rate of

$$\frac{N_{B^*}}{N_{B^*} + N_B} = (77.1 \pm 2.6 \pm 7.0)\% \tag{4}$$

is found. The systematic error of 2% on η_B is derived from the stability plot of the relative B^* production rate as a function of the b purity (Fig. 4b). Several studies were done to determine the systematic uncertainty of the photon efficiency:

- The agreement of the total conversion rate between data and Monte Carlo (see Fig. 2d) is $[0.1 \pm 0.5(stat.)]\%$. The systematic uncertainty of the photon efficiency due to a different material distribution or reconstruction efficiency for converted photons in data and Monte Carlo is estimated to be 2% from studies using the well known TPC gas to normalize the conversion rate.

- The normalization factor for the background from the Monte Carlo simulation obtained in the sideband region ($M(B\gamma) - M(B) < 0.02$ GeV/c^2, $0.08 <$ M(Bγ) $-$ M(B) $<$ 0.2 GeV/c^2) of the B^* signal is found to be 1.020 ± 0.008. This 2% deviation from unity can have its origin either in a wrong B tagging efficiency, a wrong π^0 production rate or a wrong photon reconstruction efficiency in the Monte Carlo simulation. The B tagging efficiency is checked in data and Monte Carlo by comparing the number of single and double tagged events (N_t and N_{tt}). The result is $(2N_{tt}/N_t)^{data}/(2N_{tt}/N_t)^{MC} = 1.01 \pm 0.01$. To be conservative the 2% deviation from unity in the background

Error source	Absolute error on $N_{B^*}/(N_{B^*}+N_B)$
Monte Carlo weighting	3.9%
Monte Carlo statistics	2.4%
b purity	1.6%
γ efficiency	2.3%
f_B	3.8%
Variation of all cuts	2.5%
total (quadratic sum)	7.0%

Table 2: Contributions to the systematic error on the relative B^* production rate.

normalization is assigned as a systematic error on the photon detection efficiency since a wrong π^0 production rate in the Monte Carlo simulation would not effect the extracted B^* production rate.

- The reconstruction efficiency for converted photons is energy dependent (see Fig. 2c). Therefore a variation of the B^*-B mass difference changes the photon efficiency. In order to estimate this effect the B^*-B mass difference was varied in the Monte Carlo simulation by ± 1 MeV/c^2. The resulting uncertainty in the photon efficiency is $\pm 1\%$.

A complete breakdown of the quoted systematic error is given in Table 2. All cuts applied in this analysis are varied within reasonable ranges and the variation of the result is included in the systematic error.

5.2 B^* Polarization

The decay angle of the photon in the B^* rest frame θ^* can be used to distinguish between transverse (helicity ± 1) and longitudinal (helicity 0) polarized B^* mesons, which have the differential cross sections $\sigma_T \propto (1+\cos^2\theta^*)/2$ and $\sigma_L \propto \sin^2\theta^*$ respectively. If the helicity states are equally populated, i.e. $\sigma_T : \sigma_L = 2:1$, a flat helicity angle distribution is expected.

For this measurement the $\cos\theta^*$ range is extended down to -0.6 to increase the sensitivity. The number of B^* mesons is determined in 7 bins of $\cos\theta^*$. The efficiency-corrected result is shown in Fig. 5. The relative longitudinal contribution is determined from the fit to be

$$\frac{\sigma_L}{\sigma_L+\sigma_T} = (33 \pm 6 \pm 5)\%, \tag{5}$$

in agreement with the expectation of 1/3 for equally populated helicity states. The systematic error reflects the uncertainty on the photon efficiency as a function of the photon energy, which is highly correlated with $\cos\theta^*$.

6 The decay $B^{**}_{u,d} \to B^{(*)}\pi^{\pm}$

For the B^{**} search, the photon is replaced by a charged pion. This pion is called in the following π^{**}. The photon from the decay $B^{**} \to B^*\pi^{\pm}, B^* \to B\gamma$ is lost. Only a small

fraction of B^* mesons ($\approx 10\%$) are expected to originate from B^{**} decays. Therefore the search for B^{**} states starting with a reconstructed $B^* \to B\gamma, \gamma \to e^+e^-$ decay would reduce the signal by a large factor but not affect the background level. Also no improvement for the signal width is expected, due to the fact that the photon is of such low energy compared to the π^{**} in the B^{**} rest frame that the photon lost in the decay chain only shifts the effective mass of the $(B\pi^{\pm})$ system down by 46 MeV/c^2 from the true B^{**} mass, but does not broaden the signal significantly.

The B^{**} has a negligible lifetime compared to the average B hadron. This allows to reduce the combinatorial background using the signed impact parameter to distinguish between tracks from the primary vertex and tracks originating from the long lived B hadron decay. In order to be able to assign charged tracks with high purity to either the primary- or the B decay vertex, jets are selected which have a probability of $\mathcal{P}_J \leq 1.6 \cdot 10^{-6}$ to contain no long lived hadron and a reconstructed B hadron with a momentum of more than 25 GeV/c. In addition strict track selection cuts for the π^{**} candidates are applied:

- to have at least 10 TPC hits and at least 1 VDET hit,
- to originate from a cylindrical region of 1 cm radius and length 2 cm centered around the interaction point,
- to have a χ^2 per degree of freedom from the track fit of less than 5 and to have a momentum of more than 1.5 GeV/c,
- to have a dE/dx measurement in the TPC which is consistent with a pion (probability $> 30\%$),
- to have a probability of $|\mathcal{P}_T| \geq 0.3$ to originate from the primary vertex,
- to be in a cone around the reconstructed B hadron direction of 26 degree.

In the Monte Carlo simulation, B^{**} mesons were generated with mass differences relative to the B meson between 500 and 800 MeV/c^2 and reconstructed within 1σ (statistical error only) of the nominal value.

The distribution of the $B\pi^{\pm}$-B mass difference obtained from the 1991–1994 ALEPH data is shown in Fig. 6a. The background is estimated from the Monte Carlo simulation and normalized in the sideband regions ($M(B\pi) - M(B) < 0.25$GeV/c^2, $0.7 <$ M(Bπ) $-$ M(B) $<$ 1.2GeV/c^2) of the B^{**} signal.

As is shown in Ref. [15] the JETSET 7.3 [9] modeling of the pion spectrum from B decays is poor for pions which are soft in the B rest frame. In the low ΔM region these soft pions account for a sizable fraction of the background (see Fig. 6a). Therefore the Monte Carlo data as shown in Fig. 6 are reweighted according to the observed difference between the inclusive pion spectrum from B decays as measured by ARGUS [15] and that generated in the ALEPH Monte Carlo. As can be seen from Fig. 6a the shape of the background is reproduced well on both sides of the signal after this procedure.

The background-subtracted signal is fitted by a simple Gaussian. A resonance structure in the $M(B\pi) - M(B)$ distribution is observed at

$$M(B\pi) - M(B) = (424 \pm 4 \pm 10) \text{ MeV/c}^2. \tag{6}$$

It has a width of

$$\sigma(\Delta M) = (53 \pm 3 \pm 9)\ \mathrm{MeV/c^2} \tag{7}$$

and the number of reconstructed B^{**} decays to $B^{(*)}\pi^{\pm}$ is

$$N(B^{**}) = 1944 \pm 108 \pm 161. \tag{8}$$

The shape and the normalization of the background is the dominant source for the quoted systematic errors. To estimate them the following studies are performed:

- The Monte Carlo data are reweighted according to the observed difference in the reconstructed B momentum spectrum (Fig. 1d). The effect is negligible.
- The Peterson fragmentation parameter ϵ_b is varied in the range $0.004 - 0.008$ in the Monte Carlo simulation. This changes the yield by ± 62 events and has no effect on ΔM or $\sigma(\Delta M)$.
- The limited Monte Carlo statistics of 3.6 million hadronic Z events and the normalization of the background in the sideband region of the B^{**} signal account for a systematic error of ± 151 on the yield, of ± 2 MeV/c^2 on ΔM, and of ± 4 MeV/c^2 on $\sigma(\Delta M)$.
- The complete analysis is repeated several times with different sets of B- and π^{**}-selection cuts. The minimum B momentum cut is varied from 20 to 30 GeV/c, the jet selection cut $\mathcal{P}_J$ in the range $5 \times 10^{-3} - 5 \times 10^{-8}$, the minimum momentum cut for π^{**} from 0.5 to 2 GeV/c, and the cut on $\mathcal{P}_T$ in the range $0.2 \leq |\mathcal{P}_T^{cut}| \leq 0.4$. Finally, in order to study the influence of the unknown helicity structure of the B^{**} states, the π^{**} candidate sample is divided in two helicity bins, $\cos\theta^*_{\pi^{**}} \geq 0$ and $\cos\theta^*_{\pi^{**}} < 0$, which leads to the dominant systematic error on ΔM. The quoted systematic errors on $M(B\pi) - M(B)$ and $\sigma(\Delta M)$ correspond to half of the observed variation in each case. The relative systematic error on the π^{**} efficiency estimated from these studies is 1.5% (Table 3).

6.1 B^{**} Mass and Production Rate

The fitted signal width is larger than the detector resolution of 40 MeV/c^2. It is interpreted as a superposition of several B^{**} states and/or decay modes as observed for the P-wave D meson states [3] and as predicted for the excited B states [5]. Possible contributions of B_s^{**} decays into $B_{u,d}K^{\pm}$, with the kaon misidentified as a pion, are expected from a Monte Carlo simulation to be only of the order of 2%. They are considered for the $B_{u,d}^{**}$ production rate.

In order to arrive at a $B_{u,d}^{**}$ mass value and production rate, assumptions must be made on the relative production rates and decay modes of the four different expected $B_{u,d}^{**}$ states. Following spin counting arguments and heavy quark effective theory [16], the relative production rates are expected to be $B_1 : B_0^* : B_1^* : B_2^* \equiv 3 : 1 : 3 : 5$. A model based on the predictions for the narrow $B_{u,d}^{**}$ states (see Table 1) from Ref. [5], i.e., $M(B_2^*) - M(B_1) = 12$ MeV/c^2, $BR(B_2^* \to B\pi) = BR(B_2^* \to B^*\pi) = 50\%$, $BR(B_1 \to B^*\pi) = 100\%$ and $\Gamma(B_2^*) \approx \Gamma(B_1)$ is used to describe the B^{**} signal.

For the fit procedure the yield, the mass, and the width of the B_2^* state are taken as free parameters while the detector resolution is fixed according to the Monte Carlo

expectation. The following numbers are obtained (see Fig. 7a): $N(B^{**}) = 2049 \pm 133$, $M(B_2^*) = (5741 \pm 3)$ MeV/c^2 and $\Gamma(B_2^*) = (21 \pm 11)$ MeV/c^2. The quoted errors are statistical only. The large theoretical uncertainties do not allow to quote any meaningful systematic error with the current experimental resolution. The sensitivity to the width of the B_2^* state is small since the signal width is dominated by the detector resolution of 40 MeV/c^2. The width is in agreement with the expectation of 24 MeV/c^2 from Ref. [5]. The signal is therefore interpreted as arising from the decays of the narrow $B_{u,d}^{**}$ states.

However the relative production rates, masses and widths of the broad $B_{u,d}^{**}$ states are unknown. Their possible contribution to the signal has to be estimated in order to calculate a $B_{u,d}^{**}$ production rate. Attempts to constrain the masses and widths of the broad $B_{u,d}^{**}$ states from the experimental data were not successful. A resonance structure with an intrinsic width of a few hundred MeV/c^2 could not be separated from a Monte Carlo estimate of the background with the procedure used in this analysis. On the other hand broad $B_{u,d}^{**}$ states with width and mass splitting relative to the narrow $B_{u,d}^{**}$ states of for example 70 MeV/c^2 (see Fig. 7b) and a production rate following spin counting can not be excluded with the observed signal. The unknown properties of the broad $B_{u,d}^{**}$ states are therefore included in the systematic uncertainty of the $B_{u,d}^{**}$ production rate.

In the notation of section 5.1, the relative $B_{u,d}^{**}$ production rate is given by

$$\frac{BR(Z \to b \to B_{u,d}^{**})}{BR(Z \to b \to B_{u,d})} = \frac{N(B^{**})\ f(B_{u,d}^{**})}{\eta_B\ N_{TAG}\ \epsilon_{\pi^{**}}\ f_{B_{u,d}}\ f_N(B_{u,d}^{**})}. \tag{9}$$

where $f(B_{u,d}^{**})$ is fraction of $B_{u,d}^{**}$ in the obtained B^{**} signal, $\epsilon_{\pi^{**}}$ is the π^{**} efficiency, $f_{B_{u,d}}$ is the fraction of $B_{u,d}$ mesons produced in $Z \to b\bar{b}$ decays estimated to be $f_{B_{u,d}} = (76.8 \pm 5.2)\%$ [14] and $f_N(B_{u,d}^{**})$ is the fraction of reconstructed narrow $B_{u,d}^{**}$ states.

From $N_{q\bar{q}} = 2,948,727$ $q\bar{q}$ events $N_{TAG} = 90,713$ B jets are selected in which $1944 \pm 108 \pm 161$ B^{**} mesons are reconstructed. The signal can be parameterized with equal goodness of fit using a single Gaussian (model I), the model for the production of narrow B^{**} states according to Ref. [5] (model II), or using a single Breit-Wigner folded with the detector resolution (model III). The value obtained using model II is closest to the number extracted from simply counting the excess in the signal region and is between the yield obtained from the other two models. It is 5% larger than the estimated number of events from the single Gaussian fit due to non Gaussian tails which are expected for most B^{**} production models. To account for the unknown signal shape a scaling factor of 1.05 ± 0.05 is therefore applied to the yield extracted from the Gaussian fit.

$f(B_{u,d}^{**})$ is estimated from the Monte Carlo simulation to be 0.98 ± 0.02. The contamination from B_s^{**} decays to $BK^{\pm}$ is small as a dE/dx probability of larger than 30% for the pion hypothesis is required for the π^{**} candidates.

The expected fraction of narrow $B_{u,d}^{**}$ states is:

- $f_N(B_{u,d}^{**}) = 1/2$: Only narrow states contribute to the signal and the production rate follows state counting.
- $f_N(B_{u,d}^{**}) = 2/3$: Only narrow states contribute to the signal and the production rate follows spin counting.
- $f_N(B_{u,d}^{**}) = 1.0$: Broad and narrow states contribute with equal efficiency to the signal.

Error source	Absolute error on $BR(Z \to b \to B^{**}_{u,d})/BR(Z \to b \to B_{u,d})$
Background normalization	2.2%
Variation of ϵ_b	0.8%
Variation of all cuts	3.9%
Signal shape	1.4%
B^{**}_s contribution	0.6%
π^{**} momentum cut	2.7%
b purity	0.6%
$\mathcal{P}(b \to B_{u,d})$	1.9%
total (quadratic sum)	5.9%

Table 3: Contributions to the systematic error on the relative B^{**} production rate.

$f_N(B^{**}_{u,d})$ can take any value between 1/2 and 1 if the reconstruction efficiency for broad and narrow $B^{**}_{u,d}$ is different. The most likely scenario corresponds to $f_N(B^{**}_{u,d}) = 2/3$ and hence $f_N(B^{**}_{u,d}) = 0.67^{+0.17}_{-0.08}$ is used in the following. The error corresponds to half of the possible spread.

The pion efficiency $\epsilon_{\pi^{**}} = (23.7 \pm 4.1)\%$ and the b purity $\eta_B = (98.5 \pm 1.5)\%$ are taken from the Monte Carlo simulation. With these numbers the following relative $B^{**}_{u,d}$ production rate

$$\frac{BR(Z \to b \to B^{**}_{u,d})}{BR(Z \to b \to B_{u,d})} = [27.9 \pm 1.6(stat) \pm 5.9(syst)\ {}^{+3.9}_{-5.6}(model)]\% \qquad (10)$$

is found. The third error reflects the uncertainty due to the unknown value of $f_N(B^{**}_{u,d})$. In this result the assumption is made that 2/3 of all $B^{**}_{u,d}$ mesons decay into charged pions and 1/3 into (unobserved) neutral pions. Possible decay modes into $B\rho$ are expected to be small due to the limited phase space.

The stability of the result is shown in Fig. 8b as a function of the b purity. Only the relative statistical errors with respect to the nominal cut are plotted. A breakdown of the total systematic error is given in Table 3. The momentum cut of 1.5 GeV/c for the π^{**} leads to an uncertainty of 10% on the π^{**} efficiency due to the fact that it is not known which $B^{**}_{u,d}$ states contribute to the observed signal.

7 Summary and Conclusions

Using the known decay $B^* \to B\gamma$, a method for the inclusive reconstruction of B hadron decays was developed. The following measurements for the B^* state are obtained

$$\frac{N_{B^*}}{N_{B^*} + N_B} = (77.1 \pm 2.6 \pm 7.0)\%, \qquad (11)$$

$$M(B^*) - M(B) = (45.30 \pm 0.35 \pm 0.87)\ \mathrm{MeV/c^2}, \qquad (12)$$

$$\frac{\sigma_L}{\sigma_L + \sigma_T} = (33 \pm 6 \pm 5).\% \qquad (13)$$

in agreement with the expectation from a spin counting picture and with the recent results from L3 and DELPHI [17]. For the B^*-B-mass difference a similar precision to the previous

measurements by CUSB2 [18] (45.4±1.0) MeV/c^2 and CLEO2 [19] (46.2±0.3±0.8) MeV/c^2 is obtained.

Combining the B hadron instead with a charged pion yields an enhancement in the $B\pi$ mass distribution. Fitting the resonance structure observed in the background subtracted $M(B\pi) - M(B)$ distribution with a simple Gaussian yields the following parameters:

$$N(B^{**}) = 1944 \pm 108 \pm 161, \quad (14)$$

$$M(B\pi) - M(B) = (424 \pm 4 \pm 10)\ \mathrm{MeV/c^2}, \quad (15)$$

$$\sigma(\Delta M) = (53 \pm 3 \pm 9)\ \mathrm{MeV/c^2}. \quad (16)$$

The observed signal is interpreted as arising from the narrow B^{**} states described in Ref. [5], although a contribution from broad states can not be excluded with the current experimental resolution. The relative $B^{**}_{u,d}$ production rate is extracted to be

$$\frac{BR(Z \to b \to B^{**}_{u,d})}{BR(Z \to b \to B_{u,d})} = [27.9 \pm 1.6(stat) \pm 5.9(syst)\ {}^{+3.9}_{-5.6}(model)]\% \quad (17)$$

where the third error reflects the uncertainty due to different production and decay models for the broad $B^{**}_{u,d}$ states. The measured mass difference and production rate is consistent with the recent results from OPAL [20] and DELPHI [21].

8 Acknowledgements

We would like to thank our colleagues of the accelerator divisions at CERN for the outstanding performance of the LEP machine. Thanks are also due to the many engineers, and technical personnel at CERN and at the home institutes for their contribution to ALEPH's success. Those of us not from member states wish to thank CERN for its hospitality.

References

[1] Particle Data Group, Phys. Rev. **D 50** (1994) 1173.

[2] D. Buskulic et al. (ALEPH Collaboration), Z. Phys. **C 62** (1994) 1.

[3] P. Avery et al. (CLEO Collaboration), Phys. Lett. **B 331** (1994) 236;
F. Butler et al. (CLEO Collaboration), "Observation of $D_1(2430)^+$ and $D_2^*(2470)^+$", contributed paper to the International Conference on High Energy Physics, Glasgow 1994, ref. gls0185;
ALEPH Collaboration, "D^{**} Production in Z Decays", contributed paper to the International Conference on High Energy Physics, Glasgow 1994, ref. gls0577;
DELPHI Collaboration, "Study of D, D^* and D^{**} Production in Z Hadronic Decays", contributed paper to the International Conference on High Energy Physics, Glasgow 1994, ref. gls0185.

[4] M. Gronau, A. Nippe and J.L Rosner, Phys. Rev. **D 47** (1993) 1988.

[5] E.J. Eichten, C.T. Hill and C. Quigg, Phys. Rev. Lett. **71** (1993) 4116.

[6] D. Decamp et al. (ALEPH Collaboration), Nucl. Instr. Meth. **A 294** (1990) 121;
G. Batignani et al. (ALEPH Collaboration), Nucl. Instr. Meth. **B 23A** (1991) 291;
D. Buskulic et al. (ALEPH Collaboration), Nucl. Instr. Meth. **A 360** (1995) 481.

[7] D. Decamp et al. (ALEPH Collaboration), Z. Phys. **C 53** (1992) 1.

[8] J.E. Campagne and R. Zitoun, Z. Phys. **C43** (1989) 469.

[9] T. Sjöstrand and M. Bengtsson, Computer Physics Commun. **43** (1987) 367.
T.Sjöstrand, in "Z physics at LEP1", Ed. G. Altarelli et al., CERN EP/89-08 (1989), Vol. 3, 259.

[10] R. Brun et al. "The GEANT3 Electromagnetic Shower Program", CERN DD/EE/84-1 (1987).

[11] D. Buskulic et al. (ALEPH Collaboration), Phys. Lett. **B 313** (1993) 535.

[12] C. Kleinwort et al. (JADE Collaboration), Z. Phys. **C 42** (1989) 7.

[13] M. Acciarri et al. (L3 Collaboration), CERN-PPE/94-53, submitted to Phys. Lett. **B**.

[14] D. Buskulic et al. (ALEPH Collaboration), "A Measurement of $|V_{cb}|$ from $\bar{B}^0 \to D^{*+} l^- \bar{\nu}_l$", CERN-PPE/95-095, to be submitted to Phys. Lett. **B**.

[15] H. Albrecht et al. (ARGUS Collaboration), Z. Phys. **C 58** (1993) 191.

[16] N. Isgur and M.B. Wise, Phys. Lett. **B 232**(1989) 13.
M.B. Wise, Procs. XVI International Symposium on Lepton and Photon Interactions, Ithaca, New York, 1993, Ed. P. Drell, D. Rubin, p.253.

[17] M. Acciarri et al. (L3 Collaboration), CERN-PPE/94-143, submitted to Phys. Lett. **B**;
P. Abreu et al. (DELPHI Collaboration), CERN-PPE/95-53, submitted to Zeit. f. Physik C.

[18] J. Lee-Franzini et al. (CUSB Collaboration), Phys. Rev. Lett. **65**, 24 (1990).

[19] D.S. Akerib et al. (CLEO Collaboration), Phys Rev. Lett. **67**, 13 (1991).

[20] R. Akers et al. (OPAL Collaboration), CERN-PPE/94-206, submitted to Zeit. f. Physik C;

[21] P. Abreu et al. (DELPHI Collaboration), Phys. Lett. **B 345** (1995) 598.

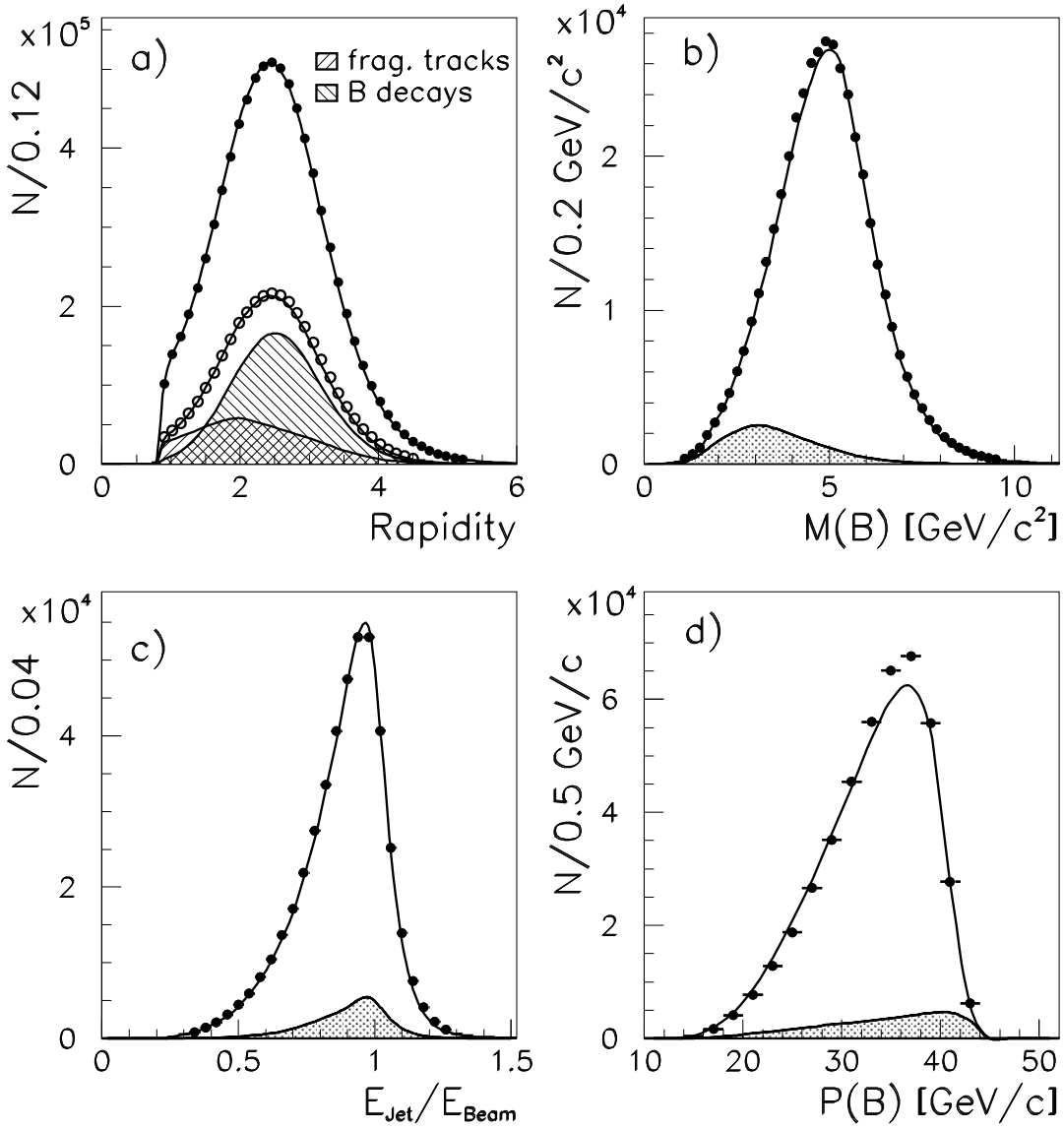

Figure 1: Comparison of data (dots) and Monte Carlo distributions (curve) normalized to the same number of $q\bar{q}$ events. (a) Rapidity distribution relative to the jet axis for all tracks (black dots) and charged tracks only (open circles). The different shape of the rapidity distributions for charged tracks from B decays and from the fragmentation process can be seen from the shaded areas. (b)–(d) Reconstructed B hadron mass, relative jet energy and B hadron momentum. The shaded area shows the background from non-$b\bar{b}$ events according to the Monte Carlo simulation.

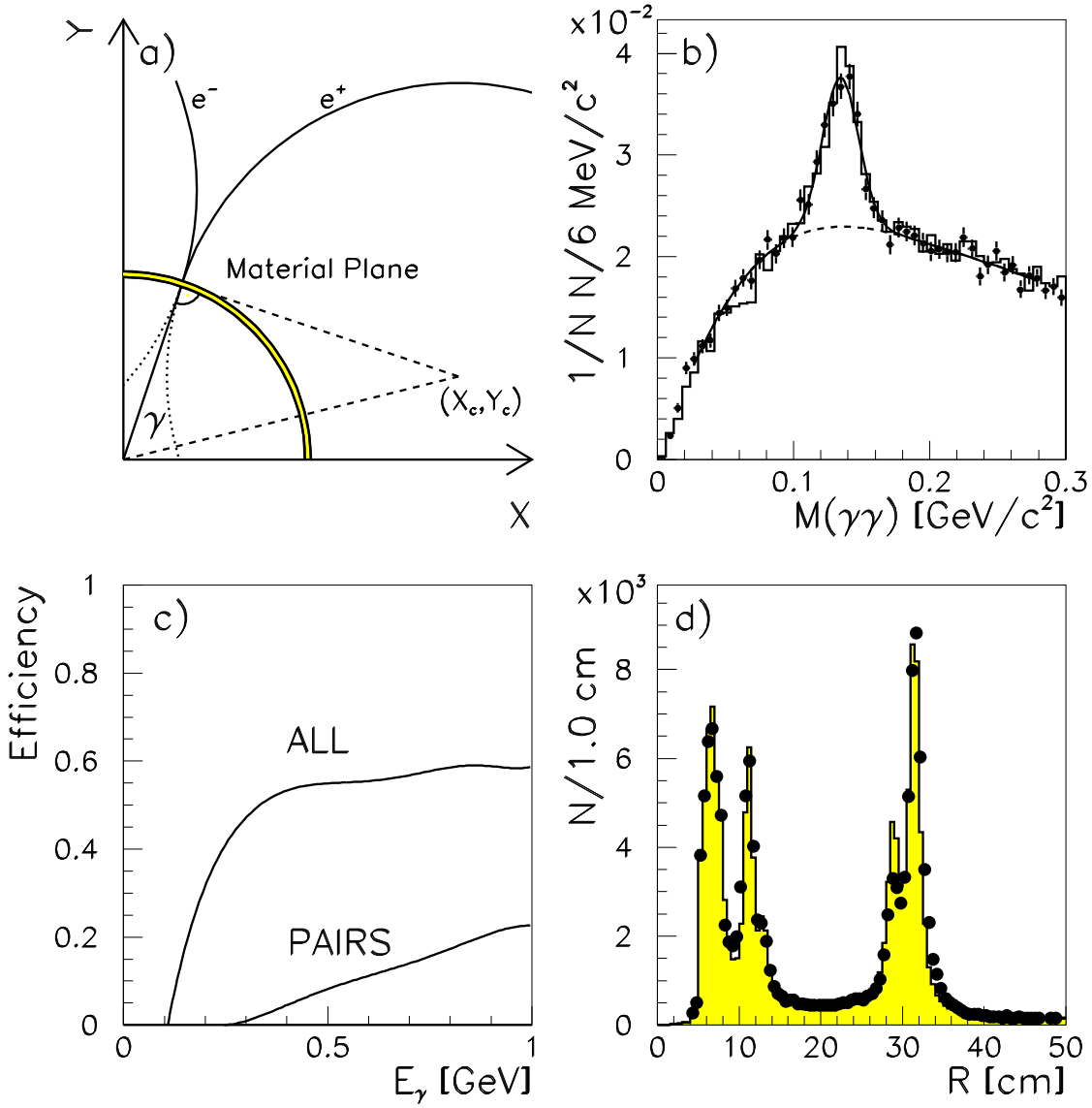

Figure 2: a) Schematic view of a photon conversion in the (X,Y)-Plane. b) Invariant $\gamma\gamma$-mass distribution from data (points) and Monte Carlo (histogram) using converted photons with the energy of one of the photons being less than 1.0 GeV. The curve shows a fit with a polynominal background and a Gaussian signal. c) Reconstruction efficiency for converted photons where the fraction of fully reconstructed conversions is indicated by the lower curve. d) Conversion radius distribution in data (points) and Monte Carlo (histogram).

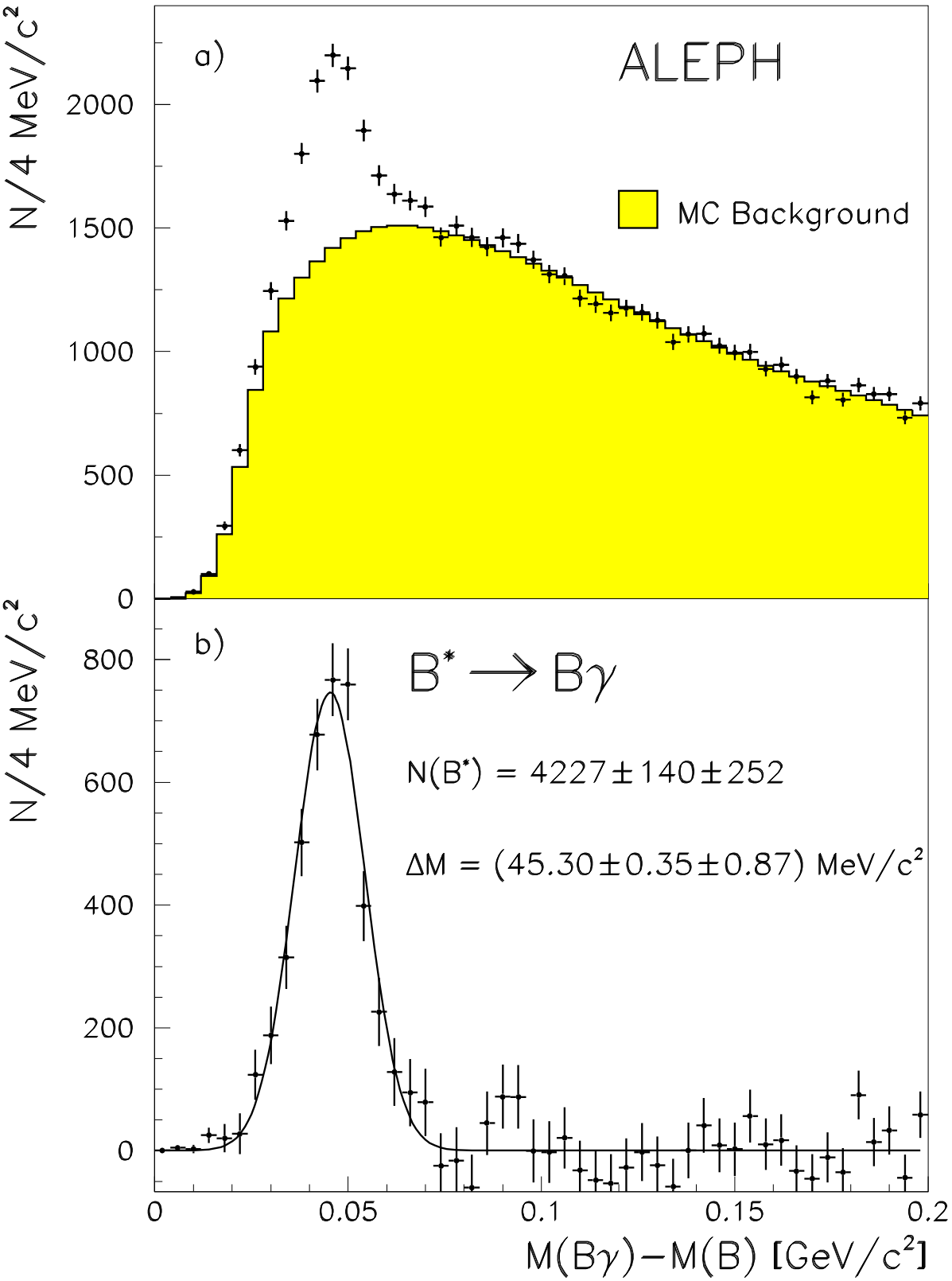

Figure 3: (a) The $B\gamma$-B-mass difference from 1991 through 1994 data using converted photons. The background estimated from the Monte Carlo simulation, normalized to the same number of $q\bar{q}$-events, is shown by the hatched area. (b) The background subtracted signal for the decay $B^* \to B\gamma$ fitted with a Gaussian (curve).

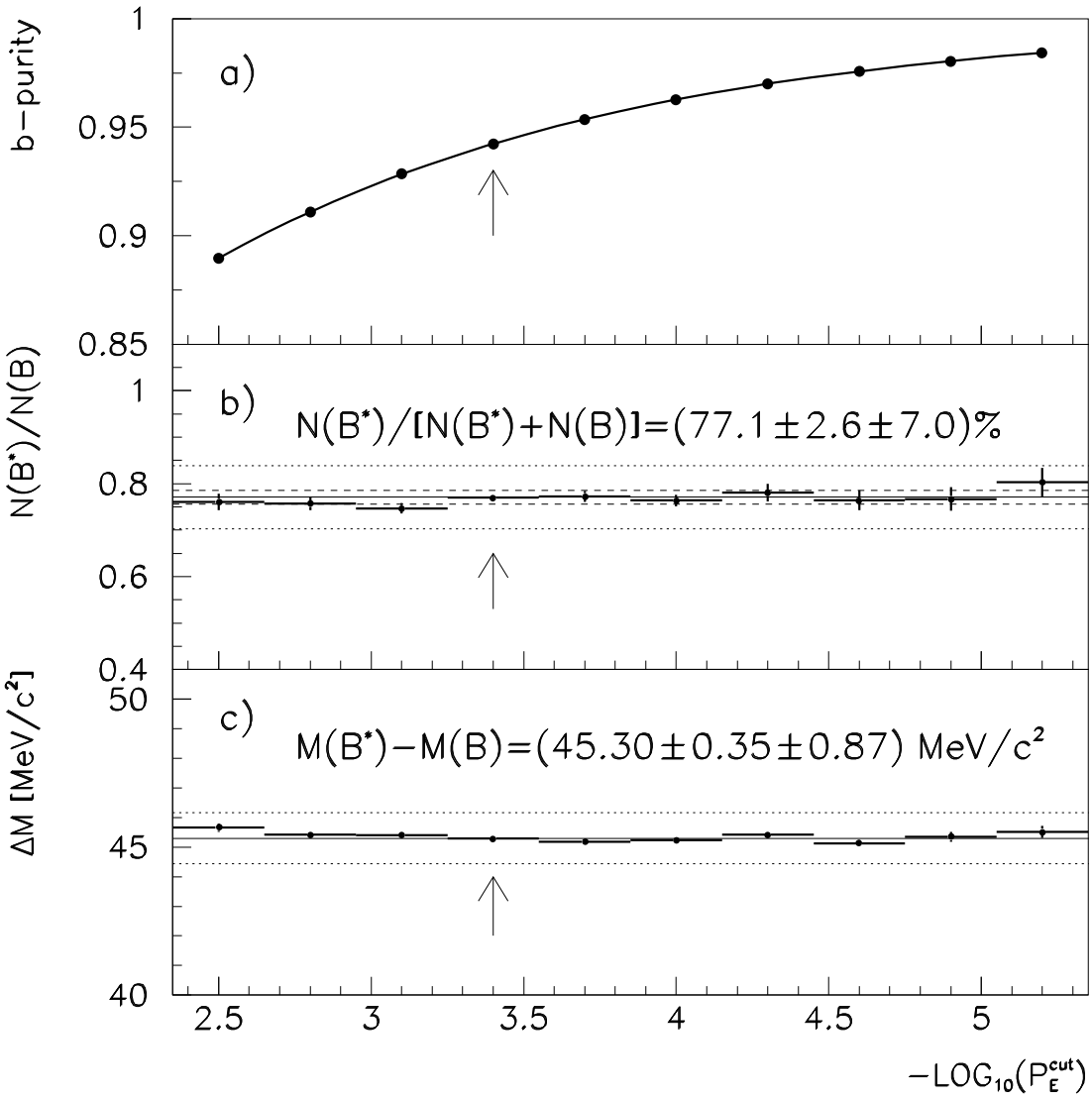

Figure 4: b purity (a), measured B^* production rate (b) and mass (c) as a function of the cut on $\mathcal{P}_E$. The dotted lines show the total systematic error. The dashed lines in (b) indicate the systematic error due to the uncertainty in the b purity.

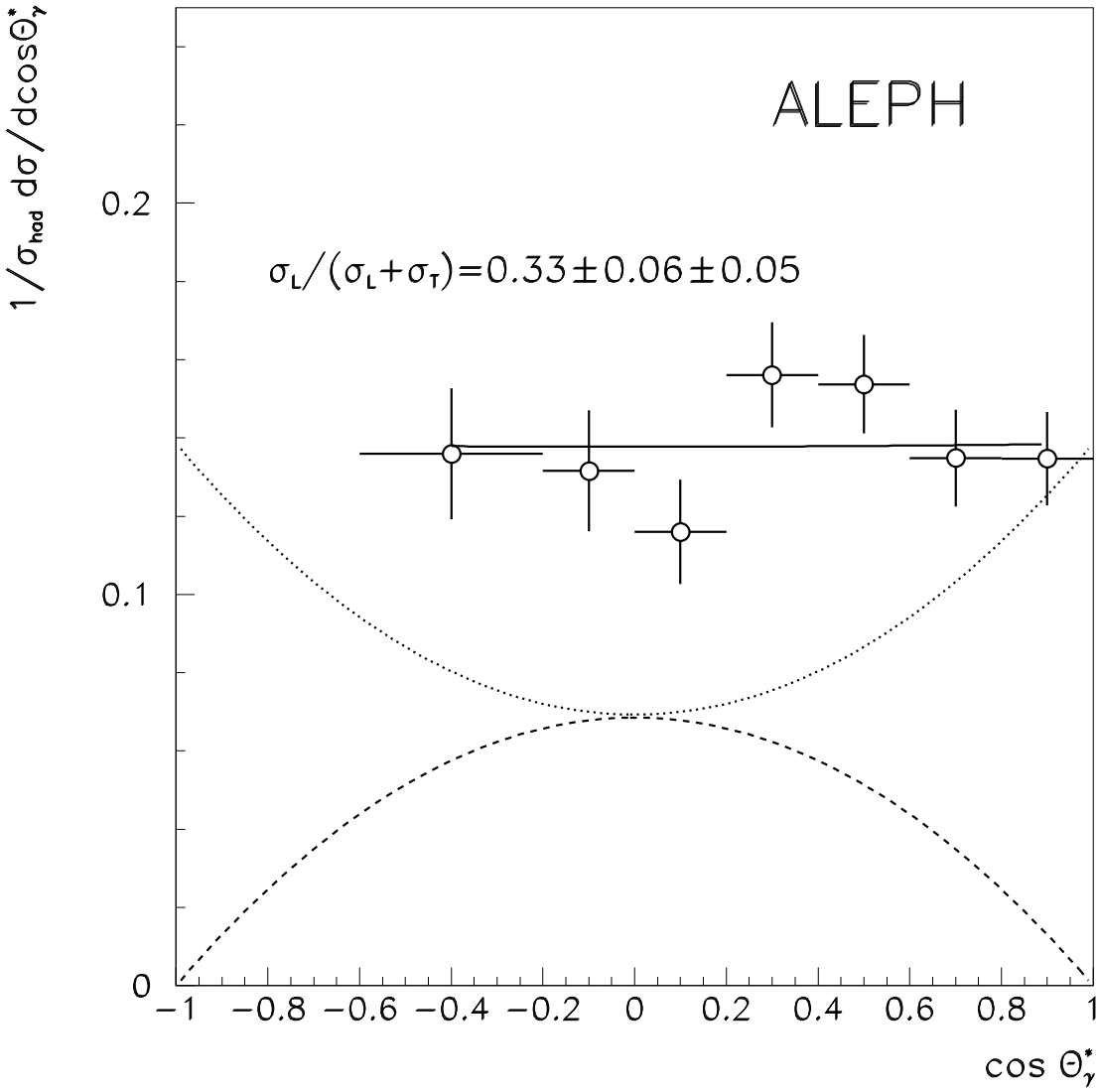

Figure 5: The acceptance-corrected number of B^*-mesons as a function of the photon decay angle ($\cos\theta^*$) in the B^* rest frame. The dashed and the dotted curves are the contributions from the transverse and longitudinal polarized states. The fit of both contributions to the data points is given by the solid curve.

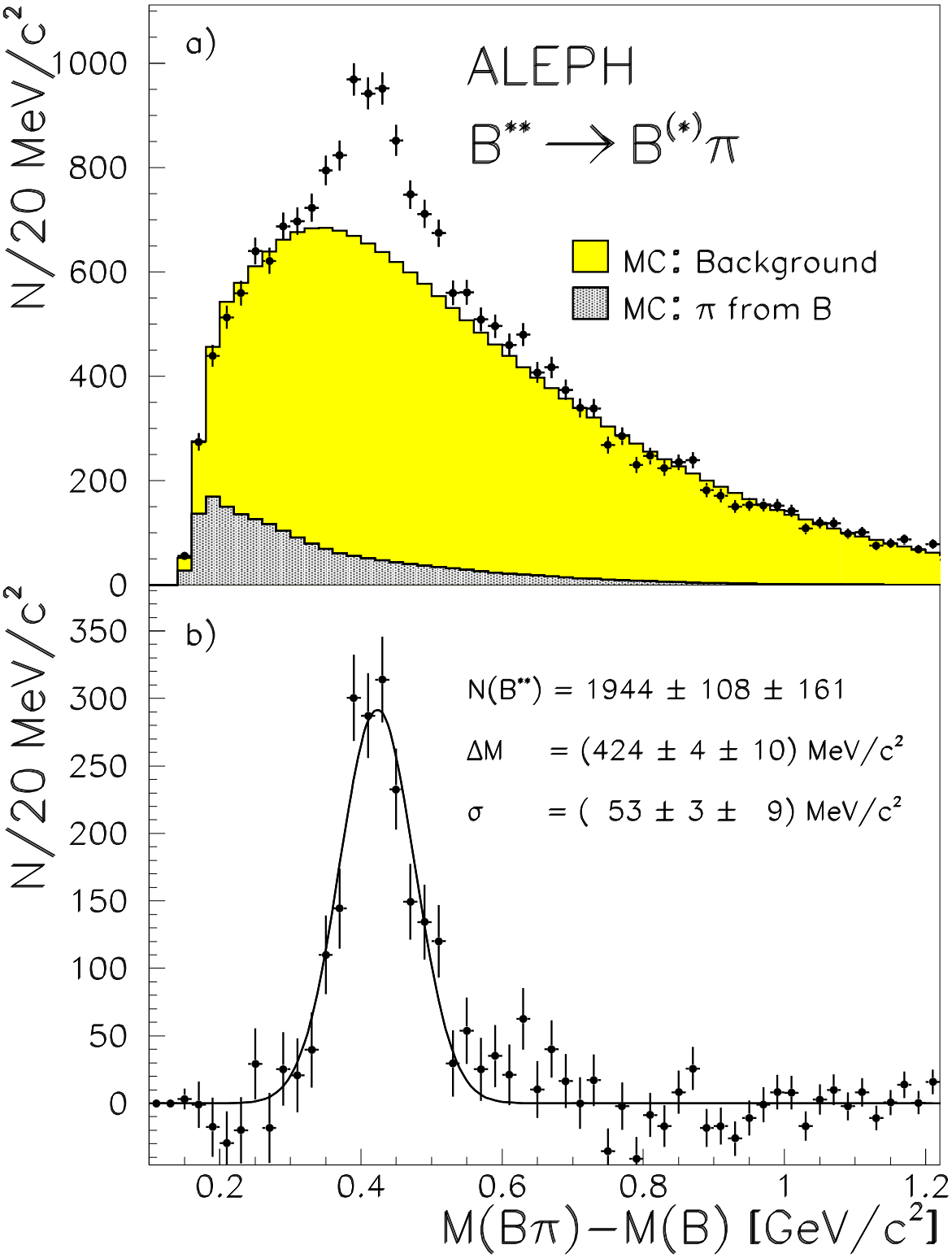

Figure 6: a) The $(B\pi) - B$-mass difference from 1991 through 1994 data. The background estimated from the Monte Carlo simulation is shown by the hatched area. (b) The background-subtracted signal for the decay $B^{**} \to B^{(*)}\pi^{\pm}$ fitted with a Gaussian (curve).

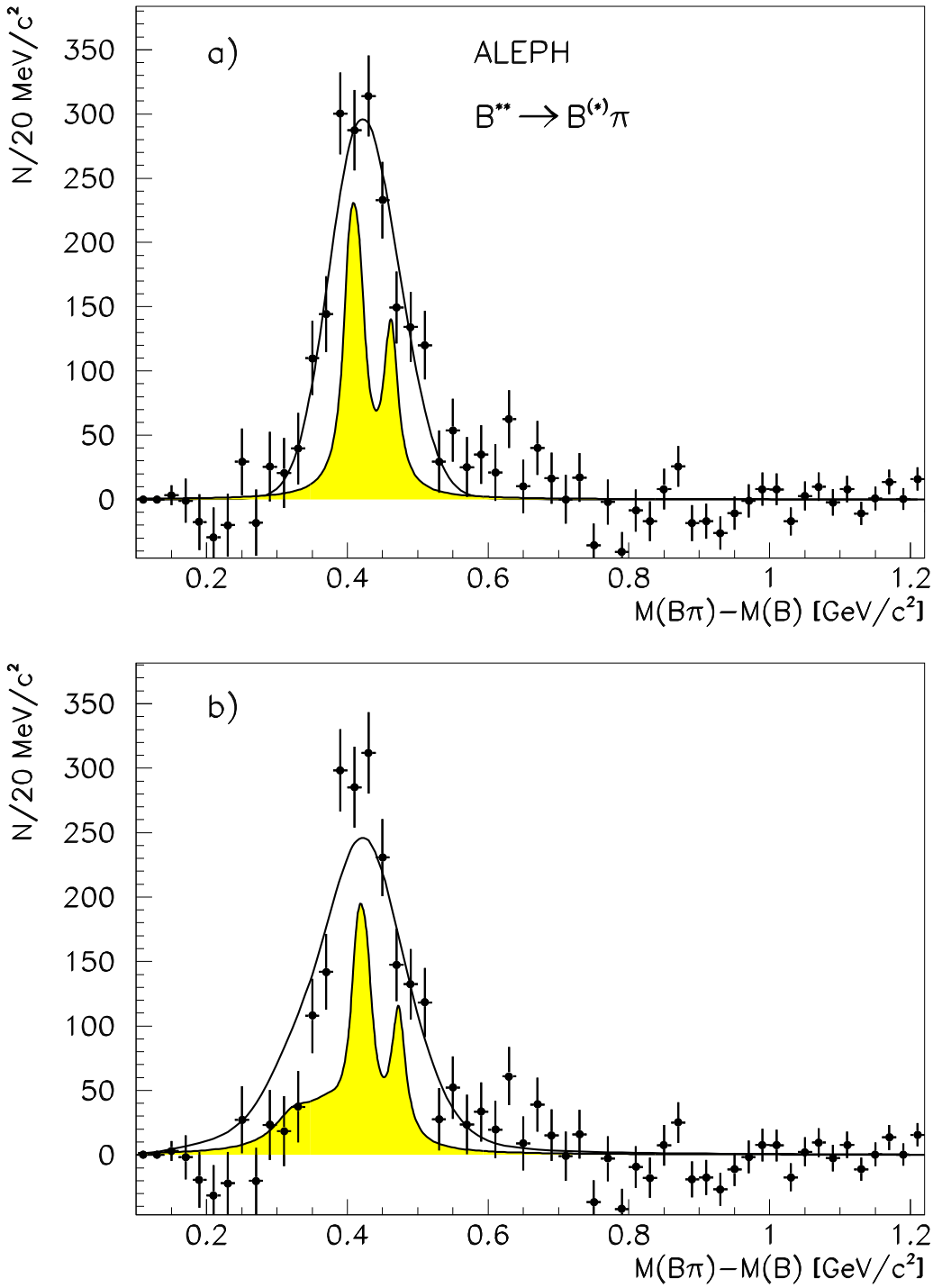

Figure 7: a) Comparison of the background subtracted B^{**} signal with the model from [5] (curve) for the narrow B^{**} states. The shaded area shows the generated structure from the two narrow $B^{**}_{u,d}$ states at an arbitrary scale. The lost photon from the B^* decay generates the double peak structure. b) The same as a) but with the additional production of broad $B^{**}_{u,d}$ states according to spin counting with a width of 70 MeV/c^2 and a mass splitting relative to the narrow states of -70 MeV/c^2.

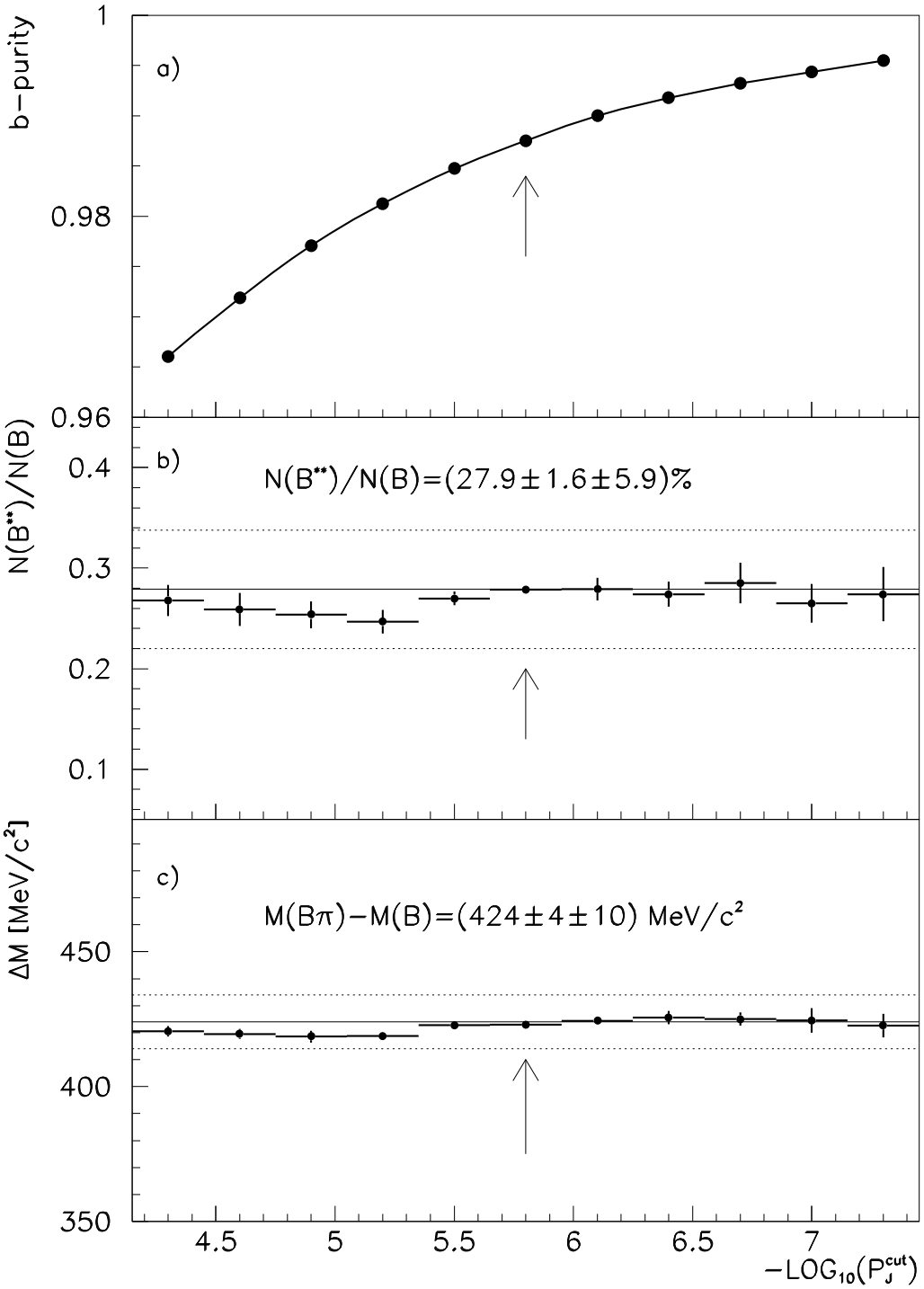

Figure 8: b purity (a), measured $B^{**}_{u,d}$ production rate (b) and mass (c) as a function of the cut on $\mathcal{P}_J$. The dotted lines show the systematic error band.